Title: Conditional *Dystrophin* ablation causes profound effects on muscle development, neurobehavior, and extracellular matrix pathways

Muthukumar Karuppasamy[1], Katherine G. English[1], James R. Conner[2], Shelby N. Rorrer[1], Michael A. Lopez[1], David K. Crossman[3], Jodi R. Paul[4], Miguel A. Monreal-Gutierrez[5], Karen L. Gamble[4], Karyn A. Esser[4], Jeffrey J. Widrick[2], Louis M. Kunkel[2,6-9], and Matthew S. Alexander[1,10-12]

[1]Department of Pediatrics, Division of Neurology at the University of Alabama at Birmingham and Children's of Alabama, Birmingham, AL 35294

[2]Division of Genetics and Genomics, Boston Children's Hospital, Boston, MA 02115, USA

[3]Department of Genetics at the University of Alabama at Birmingham, Birmingham, AL 35294

[4]Department of Psychiatry and Behavioral Neurobiology, University of Alabama at Birmingham, Birmingham, AL 35294

[5]Department of Physiology and Aging, University of Florida, Gainesville, FL 32610, USA

[6]Department of Pediatrics, Harvard Medical School, Boston, MA 02115, USA

[7]The Stem Cell Program, Boston Children's Hospital, Boston, MA 02115, USA

[8]Harvard Stem Cell Institute, Cambridge, MA 02138, USA

[9]The Manton Center for Orphan Disease Research at Boston Children's Hospital, Boston, MA 02115, USA

[10]UAB Center for Exercise Medicine at the University of Alabama at Birmingham, Birmingham, AL, 35294

[11]UAB Civitan International Research Center (CIRC), at the University of Alabama at Birmingham, Birmingham, AL 35233

[12]UAB Center for Neurodegeneration and Experimental Therapeutics (CNET), Birmingham, AL 35294, USA

Word Count: 5,872
Character Count: 34,742

Correspondence should be directed to:
Matthew S. Alexander, PhD
University of Alabama at Birmingham and Children's of Alabama
1900 University Blvd. THT 929 Box 96
Birmingham, AL 35294
Email for correspondence: matthewalexander@uabmc.edu

ORCID IDs:

Muthukumar Karuppasamy: 0000-0003-0034-9950

Katherine G. English: 0000-0003-2757-5157

James R. Conner: 0000-0002-8886-1475

Michael A. Lopez: 0000-0002-3029-0761

David K. Crossman: 0000-0002-0981-169X

Jodi R. Paul: 0000-0002-5409-5944

Miguel A. Monreal-Gutierrez: 0000-0001-8601-4080

Karen L. Gamble: 0000-0003-3813-8577

Karyn A. Esser: 0000-0002-5791-1441

Jeffrey J. Widrick: 0000-0002-5597-1141

Louis M. Kunkel: 0000-0001-6126-0242

Matthew S. Alexander: 0000-0001-7406-5171

Author Contributions: M.K., K.G.E., J.R.C., J.R.P, M.A.M-G., S.N.R., D.K.C., and J.J.W. all performed experiments for the manuscript. M.A.L. and L.M.K. contributed key resources for the manuscript. M.K. M.A.L., K.L.G., K.A.E., J.J.W., and M.S.A. wrote the manuscript. All authors approved of the manuscript prior to its submission.

Competing Interest Statement: L.M.K is a consultant for Pfizer, Dyne Therapeutics, and Myofinity for muscle disease drug therapies. All other authors declare no conflicts of interest.

Classification: Medical Sciences

Keywords: Dystrophin, DMD, muscular dystrophy, skeletal muscle, Dystrophinopathy

Abstract

Dystrophin is an essential protein for regulating the transmission of intracellular force to the extracellular matrix within the skeletal muscle. The mammalian dystrophin gene (*Dmd*) is X-linked and has several isoforms with tissue-specific expression, including the large *Dp427m* muscle transcript found in heart and skeletal muscle, and the *Dp427c* transcript that encodes the brain-specific dystrophin cerebellar protein. Dystrophin-deficiency results in Duchenne muscular dystrophy (also abbreviated DMD) in patients and understanding the pathways and tissues that are affected by dystrophin loss will impact dystrophin replacement gene therapy and exon-skipping DMD correction strategies. We generated conditional *Dystrophin* knockout mice by targeting exon 52 of the mouse *Dystrophin* (*Dmd*^{flox52}) locus. We then combinatorially generated dystrophin constitutive and inducible myofiber knockout (*Dmd* mKO; Dp427m) mice to evaluate the tissue-specific function of the large skeletal muscle dystrophin isoform (Dp427m). Constitutive embryonic deletion of the *Dystrophin* gene exclusively in skeletal myofibers resulted in a severe skeletal muscle myopathy as demonstrated using histopathology, physiological force assessments, and overall functional assessments compared to the *mdx* mouse model. Transcriptomic analysis of skeletal myofibers of the *Dmd* mKO mice revealed the dysregulation of key extracellular matrix and cytokine signaling pathways. Separately, we generated Purkinje neuron cerebellar dystrophin knockout (*Dmd*:Pcp2 KO; Dp427c) mice that displayed neurobehavioral deficits in social approach, social memory, and spatial navigation and working memory. These studies reveal the essential requirement for dystrophin within muscle development, growth, and regeneration in addition to normal neurobehavioral function.

Significance Statement

Duchenne muscular dystrophy is caused by the lack of a functional dystrophin protein in muscle. The large dystrophin (Dp427m) isoform is expressed in skeletal, cardiac, and smooth muscle, but its tissue-specific requirements remain unknown. We generated and characterized a conditional skeletal muscle knockout mouse (*Dmd* mKO). Constitutive embryonic genetic ablation of skeletal muscle *Dystrophin* resulted in muscle histopathologies similar to the *mdx* mouse, while postnatal muscle *Dystrophin* ablation resulted in milder pathologies. Ablating cerebellar *Dystrophin* Dp427c using a *Pcp2/L7*-Cre driver resulted in sociobehavioral defects. Transcriptomic analysis of the *Dmd* mKO mice showed a severe reduction of extracellular matrix and cytokine signaling

121 pathways. Our study reveals an essential role for skeletal muscle dystrophin and identifies
122 essential pathways for modulation using dystrophin-replacement therapies.
123
124 **Introduction**
125 In Duchenne muscular dystrophy (DMD) patients there is a disruption of the dystrophin gene (also
126 abbreviated *DMD*) that is predominantly expressed in skeletal and cardiac muscle. DMD patients
127 develop progressive muscle weakness in their teenage years that results in severe muscle
128 degeneration and cardiorespiratory complications. The *DMD* gene is X-linked, thus DMD
129 predominantly affects males who lose the ability to walk by their early teenage years. Mammalian
130 dystrophin protein is an essential protein that is required for normal skeletal muscle function
131 through its key binding to the actin cytoskeleton and dystrophin-associated protein complex
132 (DAPC). When fully sequenced, the human *DMD* locus was found to be extremely large as it
133 spans 2.2 megabases (Mbs) and has multiple coding regions that are essential for the function of
134 the dystrophin protein(1). The regulation of the dystrophin protein is complex in that the major
135 protein (Dp427) is expressed in multiple tissues and organs including skeletal muscle, heart, lung,
136 intestine, and the brain(2). Further complexity of dystrophin transcriptional regulation exists in that
137 multiple isoforms and *DMD* promotors exist and the regulation of its expression on a tissue-
138 specific manner has yet to be fully elucidated.
139
140 The most widely used Duchenne mouse model is the *mdx* mouse, which harbors an *Dmd* exon
141 23 nonsense mutation (C>T) at nucleotide 3185 of the large *Dp427m* RNA transcript(3, 4). Several
142 other N-ethyl-N-nitrosourea (ENU) mutagenesis and targeted knockout mouse strains have been
143 generated since the identification of the *mdx* mouse, that all show varying muscle phenotypes
144 based on the DMD mutation type and *Dystrophin* exon(s) targeted(5). Additional DMD mouse and
145 other animal models have been generated and assessed for their dystrophin expression, mutation
146 location, muscle pathophysiologies, and their ability to respond to pre-clinical and clinical
147 corrective drugs. Attempts to generate conditional mouse models have had mixed outcomes due
148 the large *DMD* gene loci and difficulties in targeting the X chromosome using gene editing. One
149 study demonstrated that a dual *Dmd* exon 2 and 79 floxed mouse when mated with a tamoxifen-
150 inducible cardiac and skeletal muscle *MerCreMer* transgene resulted in 25-35% dystrophin gene
151 excision(6). A previously homologous recombination (HR)-established knockout mouse targeting
152 dystrophin exon 52 (a known DMD mutation “hot spot” region) resulted in the disruption of the
153 large Dp427, Dp260, and Dp140 dystrophin isoforms(7). This dystrophin exon 52 model (*mdx52*)
154 displayed severe muscle degeneration pathologies, in addition to cardiac and neurobehavioral

155 defects similar to those observed in the *mdx* (*Dmd* exon 23) mouse(7-10). Using this knowledge,
156 we generated a conditional-ready *Dmd* mouse by inserting loxP sites flanking *Dystrophin* exon 52
157 (Dmd^{flox52}) that allowed for the ablation of the large *Dp427* isoforms upon Cre-mediated excision.
158 Combinatorial mating with skeletal myofiber and brain transgenic lines allowed us to define the
159 tissue-specific requirements of the dystrophin protein in skeletal muscle in early and post-natal
160 muscle growth and regeneration.
161

162 **Results**

163 ***Generation and initial characterization of skeletal muscle Dystrophin knockout mice***

164 We performed CRISPR-targeting of the mouse *Dystrophin* exon 52 locus and inserted two loxP
165 sequences in the intronic region immediately flanking the exon (**Figure 1A**). Upon Cre-mediated
166 excision of *Dmd* exon 52, the resulting DNA sequence contains an out-of-frame deletion that
167 impairs the stability of the Dp427, Dp260, and Dp140 transcripts as has been previously shown
168 in the *mdx52* mouse(11). We mated male $Dmd^{flox52/Y}$ mice with the constitutive human skeletal
169 actin (*HSA*)-Cre to ablate expression of the large Dp427m protein within the skeletal myofibers
170 (**Figure 1B**). We compared our conditional dystrophin knockout mouse model to the mdx^{5cv}
171 mouse that has well-characterized dystrophic histological, molecular, and physiological muscle
172 symptoms(12). The resulting $Dmd^{flox52/Y}$:HSA-Cre+ (*Dmd*:HSA KO) mice have no overt
173 pathologies at birth, but similar to many *mdx* strains develop a progressive muscle degeneration
174 starting between 4-6 months of age (**Figure 1C**). Analysis of both fast twitch *Tibialis anterior* (TA)
175 and slow twitch (soleus) muscles from *Dmd*:HSA KO mice showed increased centralized
176 myonuclei, large areas of fibrosis, and increased collagen production throughout the myofibers
177 (**Figure 1C**). *Dmd*:HSA KO diaphragm muscle also revealed hallmark muscle degeneration,
178 increased centralized myonuclei, and the presence of collagen deposits compared to Cre-
179 controls (**Figure 1C**). Cross-sectional area (CSA) of *Dmd*:HSA KO TA myofibers showed an
180 increased frequency of smaller myofibers compared to Cre- controls and similar to those found in
181 our mdx^{5cv} mice (**Figures 1D and 1E**). Quantitative western blot assessments of Dp427m protein
182 levels in the *Dmd*:HSA KO TA and soleus muscles showed an average of <5% remaining Dp427m
183 protein in the TA and the soleus muscles (**Figure 1F**). This was further confirmed using

184 immunofluorescent antibody staining in these muscles showing severely reduced levels of the
185 large Dp427m protein (**Supplemental Figure S1**).
186
187 **Skeletal myofiber loss of muscle dystrophin greatly impairs muscle physiological function**
188 We performed a muscle functional analysis of the *Dmd*:HSA KO adult mice by performing an
189 assessment of muscle performance following TREAT-NMD standard operating procedures
190 (SOPs) for *mdx* mice(13). *Dmd*:HSA KO mice showed reduced rotarod latency to fall, open field
191 test (OFT) total distance travelled, and impaired forelimb grip strength (**Figures 2A-2C**). All of
192 these locomotor and muscle strength metrics were comparable to those of aged-matched *mdx*
193 mice. *Dystrophin*-deficient mice have impaired treadmill running performance due in part to the
194 lack of sarcolemma-associated neuronal NOS (nNOS) binding to Dp427 at the spectrin-like
195 repeats encoded by *Dmd* exons 45-48(14, 15). We performed a standardized treadmill downhill
196 running assessment of age-matched male WT, mdx^{5cv}, $Dmd^{flox52/Y}$ (Cre negative), and *Dmd*:HSA
197 KO mice. The *Dmd*:HSA KO and mdx^{5cv} mice performed similarly in showing quicker times to
198 exhaustion, reduced overall distance travelled, and reduced velocity compared to internal cohort
199 control mice (**Figures 2D-2F**). These findings are consistent with the requirement of nNOS-
200 binding to skeletal muscle dystrophin as essential for skeletal muscle exercise and running
201 performance(16, 17). We assessed physiological force in EDL muscles from our *Dmd*:HSA KO
202 mice to determine if there were functional deficits in the peak force and resistance to high
203 mechanical strain. Despite their greater mass (**Supplemental Figure S2A**), EDL muscles from
204 the *Dmd*:HSA KO mice attained similar peak force as EDL's from the $Dmd^{flox52/Y}$ Cre- controls
205 (**Supplemental Figure S2B**). This reduction in force per unit physiological cross-sectional area
206 of muscle (**Supplemental Figure S2C**) indicates a reduction in the quality of the *Dmd*:HSA KO
207 EDL. Eccentric contractions reduced force of muscles from both groups of mice but this response
208 was exacerbated in the *Dmd*:HSA KO mice (**Supplemental Figures S2D and S2E**). These results
209 suggest that skeletal muscle Dystrophin loss has a moderate reduction in myofiber force output
210 and resistance to mechanical strain in comparison with that of *mdx* mice.
211
212 ***Dystrophin* myofiber KO mice have impaired skeletal muscle regeneration following injury**
213 We performed a cardiotoxin (ctx)-induced injury to the TA muscles of the *Dmd*:HSA KO and control
214 $Dmd^{flox52/Y}$ mice to evaluate the regenerative capacity of the skeletal muscle in the absence of the
215 Dp427m protein. The *Dmd*:HSA KO mice showed a significant amount of fibrosis, collagen, and
216 necrotic regions within the muscle that was comparable to the mdx^{5cv} strain (**Supplemental**
217 **Figure S3A**). Immunofluorescent analysis of the myofibers from the *Dmd*:HSA KO mice showed

218 elevated levels of centralized myonuclei after 21 days post ctx-injury (**Supplemental Figure**
219 **S3B**). These results demonstrate the absolute requirement for the dystrophin protein in the
220 myofiber and suggest that dystrophin from the muscle satellite cells (MuSCs) cannot compensate
221 for the lack of myofiber dystrophin in the normal regenerative process.
222
223 **Skeletal muscle-specific *Dystrophin* loss results in cytokine and ECM pathway disruption**
224 We performed RNA-sequencing on the *Dmd*:HSA KO and Cre- control TA muscles to determine
225 what transcript and signaling pathways were disrupted upon the loss of skeletal muscle
226 *Dystrophin* (**Figure 3A**). Ingenuity Pathway Analysis of RNA transcripts revealed several
227 inflammatory cytokine transcripts that were disrupted as well as extracellular matrix (ECM)
228 including several *Collagen* isoforms (**Supplemental Figure S4**). Interestingly, several transcripts
229 known to be disrupted in DMD patients were also disrupted in the *Dmd* HSA KO mice including
230 an elevation of inducible nitric oxide synthase 2 *(iNos*; *Nos2*) (**Figure 3D**). We noted a strong
231 downregulation in key immune-responsive cytokines including *Tgfb1* which drives DMD muscle
232 pathologies in *Dmd* HSA KO mouse muscles that indicates disruption of key cell-cell signaling
233 that occurs between the skeletal myofiber and the immune cells that reside in the muscle (**Figures**
234 **3B-3D**). These transcriptomic analysis confirms and essential transcriptomic regulation of key
235 signaling pathways that are known regulators of dystrophin pathophysiology.
236
237 **Postnatal skeletal myofiber *Dystrophin* loss impairs muscle maintenance despite**
238 **dystrophin protein stability**
239 We next sought to evaluate the role of skeletal muscle dystrophin in the regulation of adult skeletal
240 muscle maintenance and regeneration. Subsequently, we mated our conditional $Dmd^{flox52/Y}$ mice
241 to the *HSA*-MerCreMer tamoxifen-inducible skeletal myofiber Cre line to temporally ablate
242 Dp427m expression in the adult mice (**Figure 4A**). Two months after tamoxifen dosing, we
243 observed 25-30% reduction of total Dp427m protein within the TA skeletal muscles of *Dmd*:HSA-
244 MerCreMer+ (+ Tam) of *Dmd*:HSA-MerCreMer+ (-Tam) controls (**Figure 4B**). We observed a
245 similar 20-30% decrease of total Dp427m protein within the gastrocnemius and soleus muscles
246 in the *Dmd*:HSA-MerCreMer+ (+ Tam) mice (**Figure 4B**). These results are similar to the other
247 reported conditional *Dmd* mice that showed partial reduction of Dp427mprotein and highlights the
248 stability of the large dystrophin protein after 2 months of protein turnover(6). A histological
249 examination of the *Dmd*:HSA-MerCreMer+ (+ Tam) mice showed minimal myofiber degradation
250 and small pockets of regenerating myofibers compared to controls (**Figure 4C**). Overall myofiber
251 cross-sectional area (CSA) and minimal Feret diameter analysis revealed smaller clusters of

252 myofibers in the *Dmd*:HSA-MerCreMer+ (+ Tam) mice compared to no tamoxifen mock controls
253 (**Figures 4D and 4E**). These findings implicate the large amount of stability of the large dystrophin
254 Dp427m protein and implicate protein turnover as an essential part of dystrophin-restoration
255 therapies.
256

257 **Loss of cerebellar dystrophin impairs neurobehavioral function and results in ASD-like**
258 **behaviors**

259 Previous studies from our lab and others in various *mdx* strains demonstrated that the Dp427
260 cerebellar dystrophin isoform was essential for normal neurobehavior and social development(18-
261 21). We mated the conditional $Dmd^{flox52/Y}$ mice to *L7/Pcp2*-Cre (*Dmd*:Pcp2 KO) mice to ablate the
262 Dp427c protein in Purkinje neurons of the cerebellum (**Figure 5A**). Isolated cerebellums from
263 adult *Dmd*:Pcp2 KO mice showed loss of approximately 65% of cerebellar dystrophin protein
264 compared to Cre- controls (**Figure 5B**; **Supplemental Figure S5**). We performed a series of
265 neurobehavioral assessments in the *Dmd*:Pcp2 KO mice including social approach and social
266 novelty between novel and familiar objects and mice (**Figure 5C**). *Dmd*:Pcp2 KO showed
267 impaired social novelty in object recognition compared to $Dmd^{flox52/Y}$ Cre- control mice (**Figures**
268 **5D and 5E**). We performed a similar 3-chamber assessment (novel mouse versus familiar mouse)
269 and the *Dmd*:Pcp2 KO mice showed no preference for either mouse as compared to controls
270 suggesting that social behavior defects are linked to cerebellar dystrophin protein expression. We
271 performed both T- and Y-maze assessments in the *Dmd*:Pcp2 KO mice and found no differences
272 in T-maze alternations compared to Cre- control mice (**Figure 5F**). However, in the Y-maze
273 assessment, *Dmd*:Pcp2 KO mice had reduced alternations without a change in total arm visits
274 which together suggest reduced spatial working memory compared to Cre- controls (**Figure 5G**).
275 Memory tests were also conducted on the *Dmd*:Pcp2 KO mice that displayed impaired time to
276 find the platform in Morris water maze (**Figure 5H**). These findings support an essential role for
277 cerebellar Purkinje neuronal expression of *Dystrophin* and demonstrate a functional role for
278 Dp427 in the regulation of neurobehavior in DMD.
279

280 **Discussion**

281 The generation of novel dystrophinopathy animal models using CRISPR gene editing and other
282 next-generation genomic DNA editing tools highlights the growing need for comprehensive animal
283 models that accurately reflect disease symptoms and pathophysiologies(22). Our conditional
284 dystrophin knockout model allows for the tissue-specific study of the impact of both dystrophin
285 loss and when combined with dystrophin-replacement strategies, correct DMD strategies. Newer

286 dystrophinopathy mouse models have identified the impact of dystrophin loss on muscle disease
287 symptom progression. The *bmx* (Becker muscular dystrophy; *Dmd* exons 45-47 in-frame deletion)
288 mouse has been useful in elucidating the slower muscle disease progression that occurs in
289 patients(23).
290
291 Previous attempts to delineate skeletal muscle dystrophin protein expression using AAV-shRNAi
292 strategies have revealed dystrophin as essential for sarcomeric organization within the muscle
293 myofiber(24). A study of cultured *mdx* mouse myoblasts revealed a similar downregulation of
294 Collagen and histone transcripts along with impaired fusion and proliferation markers(25). Indeed,
295 there may be a significant amount of epigenetic remodeling that occurs which was shown in
296 embryonic stem (ES) cell cultures of *mdx* mice and human induced pluripotent stem cells
297 (hiPSCs)(26, 27). Given the alteration of myogenic determinant transcriptional pathways,
298 consideration of the impact of *Dystrophin* loss on epigenetic influences on myogenic
299 differentiation is warranted(28). Key autophagy and PTEN/AKT pathways have been shown to be
300 targets for therapeutic amelioration of dystrophic muscle pathologies(29-31). Questions remain
301 on the impact and influence of the large dystrophin muscle isoform on muscle satellite cells
302 (MuSCs) and its regulation of cellular polarity(32, 33). The Dp427 protein is expressed in muscle
303 satellite cells and it is currently unclear if restoration of dystrophin expression in the MuSC
304 population could compensate for myofiber dystrophin loss. Therapies to restore MuSC polarity in
305 DMD MuSCs may be beneficial for restoring the cellular kinetics and polarity defects observed in
306 DMD muscles(34, 35).
307
308 It is evident that the expression of dystrophin protein does occur in the brain and both large and
309 smaller dystrophin isoforms likely play independent and critical neuronal functions. Clinical studies
310 have demonstrated that loss of dystrophin is important for normal neurological and
311 neurobehavioral function as up to one-third of all DMD patients are diagnosed on the ASD
312 spectrum with symptoms ranging from mild cognitive impairment to severe developmental
313 delay(36-38). Evaluation of DMD mouse models have shown impaired neurobehavioral
314 responses in memory, learning, and overall electrophysiological neuronal function(20, 39-41). Our
315 *Dmd*:Pcp2 KO mice show similar defects to those in *mdx* mice, and highlight the essential role for
316 the large brain dystrophin protein expression. These results argue that newer platforms for exon-
317 skipping drug compounds that can more effectively penetrate the blood-brain-barrier (BBB) may
318 be required for the systemic restoration of dystrophin expression(42, 43). Our study demonstrates
319 the absolute requirement for both skeletal muscle and brain dystrophin and warrants further

320 evaluation of the tissue-specific pathways impacted by dystrophin loss to ultimately ameliorate
321 dystrophic disease pathologies.
322
323 **Materials and Methods**
324 **Mice:**
325 Wild type (*C57BL/6J*; strain #000664; Jackson Labs) and *mdx*^{5cv} (*C57BL/6J*; strain #002379;
326 Jackson Labs) used in all experiments were maintained in the Alexander lab colony under
327 pathogen-free conditions. Constitutive HSA-Cre (*Acta1*-Cre; strain# 006149) and tamoxifen-
328 inducible *HSA-MerCreMer* (*HSA*-MCM; strain# 031934) were purchased from Jackson Labs (Bar
329 Harbor, ME) and maintained on a congenic *C57BL/6J* background. The *L7/Pcp2*-Cre mice were
330 originally purchased from Jackson Labs and maintained on a congenic *C57BL/6J* background
331 that had been backcrossed greater than 6 generations (strain #006207; Jackson Labs). All mice
332 had a standard Teklad Global Rodent Diet (Inotiv; West Lafayette, IN) with *ad libitum* access to
333 food and water. All mouse strains and protocols were approved by the UAB Institutional Animal
334 Care and Use Committee (IACUC) under the protocol 21393.
335
336 **Generation of conditional Dystrophin knockout mice:**
337 Conditional *Dystrophin* knockout mice *(Dmd*$^{flox52/Y}$) were generated commercially (Cyagen; Santa
338 Clara, CA) via CRISPR guide editing of genomic DNA by inserting loxP sites in the intronic regions
339 flanking mouse *Dystrophin* exon 52 using a 12.2 kb homologous recombination vector. Briefly,
340 loxP sequences 5'-ATAACTTCGTATAGCATACATTATACGAAGTTAT-3' were inserted in the
341 intronic regions flanking the mouse *Dmd* exon 52 (*Dystrophin* NCBI transcript: NM_007868.6) in
342 *C57Bl/6J* mouse ES cells (mES). Positively-targeted mouse ES cells were screened for neomycin
343 cassette (later removed via FRT-mediated recombination) and diphtheria toxin subunit A (DTA)
344 selection. After PCR based confirmation of the presence of the loxP sites and removal of the
345 neomyocin cassette, the resultant ES cell line was injected into pseudopregnant females. The
346 subsequent F_0 offspring were genotyped for presence of the loxP sites at mouse *Dystrophin* exon
347 52, and then positively-targeted males were mated to WT (*C57Bl/6*) females to generate F_1
348 offspring. All positively-targeted F_1 mice were then maintained on the *C57Bl/6* strain for
349 subsequent matings. Mice were genotyped for the *Dmd*$^{flox52/Y}$ allele using a forward primer "5-
350 TGACTGCATCTGCATACGTG-3" and reverse "5-GAAGCCTGGTAGGCACCAT-3". Using the
351 Roche Expand Long Template PCR System (MilliporeSigma; Burlington, MA; Cat# 11681842001)
352 the wild type band (2226 bp), targeted loxP conditional allele (2401 bp), and Cre-mediated
353 excised band (992 bp) were used for genotyping following the manufacturer's recommendations.

354 Later genotyping was performed commercially using Transnetyx probes (Cordova, TN). Isolation
355 of genomic DNA from TA muscles, cerebellum, and tail DNA were performed using Viagen
356 DirectPCR Lysis Reagent (Viagen Biotech; Los Angeles, CA; Cat# 102-T).
357
358 **Histology and Immunofluorescent Imaging**
359 Skeletal muscles were slowly cryofrozen as unfixed tissues in Scigen TissuePlus O.C.T.
360 Compound using an isopentane (FisherScientific; Cat# AC397221000) and liquid nitrogen bath
361 as unfixed tissues. Some muscle biopsies were placed in 30% sucrose (MilliporeSigma; Cat#
362 S0389) sink overnight at 4°C prior to the slow cryofreezing to preserve histological and protein
363 integrity. Muscles were sectioned on a Leica CM1950 cryotome at 7-10 µm thickness, and
364 specimens were placed on Fisherbrand Tissue Path Superfrost Plus Gold slides (Fisher Scientific;
365 Cat# FT4981gplus). H&E staining was performed using Hematoxylin (MilliporeSigma; Cat#
366 H9627) and Eosin Y (MilliporeSigma; Cat# 318906) solutions in a previously described
367 protocol(44). Masson's trichrome staining was performed using a Masson's Trichrome Stain Kit
368 (Polysciences, Inc; Warrington, PA; Cat# 25088-1) and picrosirius red staining was performed
369 using a Picrosirius Red Stain Kit (Polysciences, Inc; Cat# 24901-500). For immunofluorescent
370 staining, tissue slides were blocked for one hour in a solution of 10% goat serum/1xPBS and
371 incubated for one hour at room temperature using a M.O.M kit (Vector Labs; Cat# BMK-2202;
372 Newark, CA). Tissue slides were set using a VECTORSHIELD Antifade mounting medium with
373 DAPI kit (Vector Labs; Cat# H-1200-10),
374
375 **Immunoblotting**
376 Immunoblotting was performed on protein lysates using tissues that were snap frozen in liquid
377 nitrogen and were homogenized using a bead homogenizer and lysing matrix A beads (MP
378 Biomedicals; Cat# 1169100-CF) following the manufacturer's protocol. Samples were
379 homogenized in T-PER™ Tissue Protein Extraction Reagent (ThermoFisher Scientific; Cat#
380 78510) supplemented with a protease inhibitor cocktail (ThermoFisher Scientific; Cat# J61852-
381 XF). Protein lysates were quantified using a Pierce BCA Protein Assay Kit (ThermoFisher
382 Scientific; Cat# 23227), and unless otherwise stated, 50 µg of total whole cell lysate was resolved
383 on 4–20% polyacrylamide Mini-PROTEAN® TGX™ Precast Protein Gels (BioRad). Following an
384 overnight transfer onto PVDF membranes (BioRad; Cat# 1620175), samples were blocked with
385 5% BSA (RPI Corp.; Cat# A30075) and incubated with primary antibody overnight, washed 3
386 times, and incubated with secondary antibodies for 1 hour at room temperature. Membranes were
387 washed 4 times for 15 minutes with gentle rocking, before being incubated with SuperSignal™

388 West Dura Extended Duration Substrate (ThermoFisher Scientific; Cat# 34075). Membranes
389 were imaged on either a ChemiDoc MP Imaging System (BioRad) or a LI-COR Odyssey CLx
390 imager.
391
392 **Antibodies**
393 Primary antibodies used in these experiments were validated on dystrophin-deficient tissues or
394 appropriate control tissues for specificity. Primary antisera used for western immunobloting and
395 immunofluorescent labeling include: dystrophin all isoforms (Abcam; Cat# ab15277), dystrophin
396 Dys1 (Leica; Cat# NCL-DYS1), and vinculin (Cell Signaling Technology; Cat# 7076S). Secondary
397 antibodies used for western immunoblotting included anti-mouse IgG HRP (Cell Signaling
398 Technology; Cat# 7076S) and anti-rabbit IgG HRP (Cell Signaling Technology; Cat# 7074S).
399 Secondary fluorescent anti-mouse and anti-rabbit IgG fluorochrome-conjugated antibodies used
400 include: Alexa Fluor 488 (ThermoFisher Scientific; Cat# A-11001 and A-11008), Alexa Fluor 555
401 (ThermoFisher Scientific; Cat# A32727 and A32732), and DyLight 633 (ThermoFisher Scientific;
402 Cat# 35563). Fluorescently labeled sections were imaged on a Nikon A1R-HD25 Confocal
403 microscope using NIS Elements software, and later processed using Adobe Photoshop (2025
404 version).
405
406 **Tamoxifen administration**
407 We used a previously-established protocol for the *HSA*-MerCreMer strain of delivering (80 mg/kg
408 body weight) of (Z)-4-hydroxyl-tamoxifen (4-OHT) (MilliporeSigma; Cat# H7904) mixed with
409 sunflower seed oil (MilliporeSigma; Cat# S5007) via 5 daily intraperitoneal injections while
410 alternating left and right sides to avoid injection site reactions (45, 46). Control mice were given
411 equivalent IP injections of sunflower seed oil. Separate mouse cohorts were assessed at 30 day
412 intervals from days 0, 30, 60, 90, and 180 days post injection. Mice were monitored for
413 hepatotoxicity using cytochrome P450 assessments and injection site reactions after
414 administration.
415
416 **Mice locomotor and functional analysis**
417 Open field testing and mouse locomotor analysis was measured using a previously established 4
418 individual chamber sensor system protocol and data was analyzed using Ethovision XT software
419 platform (Noldus; Leesburg, VA)(47, 48). Mice were analyzed for functional analysis but were first
420 acclimated to the room and open-field chambers one day prior to activity and were given a five
421 minute additional adaptation period prior to activity recording. Mouse locomotor activity was

recorded for ten minutes with no external stimulation and the experimenter isolated in a separate room.

Physiological force assessments

Mice were anesthetized with sodium pentobarbital (80 mg/kg) delivery intraperitoneal (IP) injection. Isolated EDL muscles were suspended in a phosphate buffer equilibrated with 95% O_2, 5% CO_2 (35 °C). Muscle contractions were generated using a 150 ms, supramaximal stimulus train (200 μs pulses) with the muscle held at its optimal length (L_o) for tetanic tension. Force was normalized to physiological cross-sectional area assuming a fiber length to muscle length ratio of 0.44 as previously described(47). To evaluate the force-frequency relationship, each muscle was stimulated at frequencies ranging from 30 to 300 Hz (peak force). Fixed-end force values were expressed relative to maximal peak force and fit by a sigmoid curve. Changes in the relationships were evaluated by differences in the inflection point (K, measured in Hz) and slope (H, unitless). Muscles were then subjected to an active lengthening protocol consisting of the following sequence: one fix-end contraction, 5 lengthening (eccentric) contractions, and two fixed-end contractions. All contractions began with the muscle at L_o and were elicited with 150 ms trains at 300 Hz. The lengthening trials consisted of an initial 100 ms fixed-end contraction that allowed the muscle to rise to peak force followed by a constant velocity stretch at four muscle fiber lengths/s to a final length of 120% L_o. Force was evaluated at 95 ms of stimulation for both fixed-end and lengthening trials.

Social neurobehavior and memory experiments

Social approach was determined by placing the test mouse in the middle chamber of a 3-chamber system and determining if the mouse showed preference for a novel mouse or a novel object (round ball). The social approach protocol was adapted from our previous protocol along with other established mouse neurobehavioral assessments in autism spectrum disorder (ASD) mouse models(18, 49). Mice were evaluated over 10 minute periods after a 10 minute acclimation period in which the novel mouse and novel object were kept in blocked off chambers. Placement of the novel mouse and novel object was switched between the two side chambers between intervals, and the apparatus was cleaned between evaluations. Social novelty was determined by placing the test mouse in the center chamber and evaluating the time spent in chambers containing either an unfamiliar mouse (no previous exposure) or a familiar mouse (aged-matched littermate). The mouse was monitored over a 10 min interval after the 10 minute acclimation period, and its total movement, velocity, time spent in close interaction with familiar or unfamiliar

456 mouse were measured. T-maze and Y-maze (Maze Engineers; Skokie, IL) cohort assessments
457 were performed using previously described with video recordings captured after the mouse was
458 placed in the maze center(50, 51). Spatial memory and learning evaluation of the mouse cohorts
459 was performed using the Morris Water Maze (Noldus) from an adapted protocol previously used
460 in *mdx* mice(52, 53). Experimenter was double-blinded to treatment group and genotype of the
461 mice in each cage and de-blinded occurred after data analysis.
462
463 **Skeletal muscle injury**
464 A cardiotoxin-induced injury to the TA was performed by intramuscular injection of 40 µl of 10 µM
465 cardiotoxin (Millipore Sigma; Cat# 217503) given to adult, aged-matched male mice. The
466 contralateral TA muscle was used as a sham control and given an equivalent intramuscular
467 injection of phosphate-buffered saline (1x DPBS; Millipore Sigma; Cat# D8662) given as a control.
468 Mice were evaluated at day 0 (uninjured), 7, 14, and 21 days post cardiotoxin injury for histological
469 changes in muscle architecture and myofiber composition.
470
471 **RNA-sequencing**
472 Total RNA was extracted from TA skeletal muscles from aged-matched male mice using TRIzol
473 reagent (ThermoFisher Scientific; Cat# 15596026) for extraction following the manufacture's
474 protocol. RNA with an RNA Integrity Score (RIN) greater than 7.0 was selected for library
475 amplification. Poly A enrichment using a ribominus kit (ThermoFisher Scientific; Cat# K155002)
476 was performed on the samples. A total RNA library was amplified from approximately 200-300 ng
477 of RNA using a NovaSeq 6000 reagent kit v1.5 (Illumina; San Diego, CA; Cat# 20044417) before
478 being processed on an Illumina NovaSeq 6000 sequencer. Total reads were FASTQ files were
479 uploaded to the UAB High Performance Computer cluster for bioinformatics analysis with the
480 following custom pipeline built in the Snakemake workflow system (v5.2.2)(54). Following count
481 normalization, principal component analysis (PCA) was performed, and genes were defined as
482 differentially expressed genes (DEGs) if they passed a statistical cutoff containing an adjusted p-
483 value <0.05 (Benjamini-Hochberg False Discovery Rate (FDR) method) and if they contained an
484 absolute $\log_2$ fold change >=1. Functional annotation enrichment analysis was performed in the
485 NIH Database for Annotation, Visualization and Integrated Discovery (DAVID, v6.8) by separately
486 submitting upregulated and downregulated DEGs. Ingenuity pathway analysis (IPA) was
487 performed on the data as described(55). A p-value <0.05 cutoff was applied to identify gene
488 ontology (GO) terms and the FASTQ experimental files have been uploaded to NCBI's Gene
489 Expression Omnibus under accession number GSE284723.

490

491 **Quantitative PCR analysis**

492 Total RNA was extracted using TRIzol reagent (ThermoFisher Scientific) and the lysing matrix A
493 beads (MP Biomedicals; Cat# 1169100-CF) as described above. Approximately 1 µg of RNA was
494 then reverse transcribed using SuperScript IV First-Strand Synthesis System (ThermoFisher
495 Scientific; Cat# 18091050). Approximately 0.5 µl of sample was then mixed with using TaqMan™
496 Fast Advanced Master Mix (ThermoFisher; Cat# 4444556) following the manufacturer's protocol
497 and samples were analyzed on a QuantStudio 5 Real-Time PCR machine (ThermoFisher). The
498 following Taqman real time PCR assays (ThermoFisher Scientific) were used to amplify specific
499 transcripts: *Dmd* (exon 1, Mm03956078_s1; exons 16-17, Mm00464475_m1; exons 50-51,
500 Mm01216958_m1; exons 64-65, Mm00464520_m1), and *Actb1* (Mm02619580_g1).

501

502 **Statistical Analysis**

503 For most dual cohort comparisons, either a two-tailed student's t-test or chi-squared test for
504 normality was performed for all pairwise comparisons. For longitudinal assessments over time or
505 across multiple cohorts, a one-way analysis of variance (ANOVA) with Least Significant Difference
506 (LSD) was performed for all multiple comparisons. GraphPad Prism version 10 software
507 (Graphpad Software; San Diego, CA) was used for all statistical analyses. An *a priori* hypothesis
508 of *$p < 0.05$, **$p<0.01$, ***$p<0.001$, and ****$p < 0.0001$ was used for all reported data analyses. All
509 graphs were represented as mean +/- SEM.

510

511 **Acknowledgments and Funding**

512 We would like to thank members of the Alexander lab and UAB Center for Exercise Medicine for
513 their critical evaluation of our manuscript. We would also like to thank members of the Kunkel,
514 Gamble, and Esser labs for reviewing our manuscript and assistance with data interpretation.
515 M.S.A. is supported by NIH grants from the Office of the Director under award number
516 (U54OD030167), and an R21 grant from National Institute of Neurological Disorders and Stroke
517 (NINDS) (R21NS140497). Additional funding support was provided by the Hope4Gabe
518 foundation. L.M.K. is supported by NIH National Institute of Arthritis and Musculoskeletal and Skin
519 Diseases (NIAMS) grant R01AR064300, and the Bernard F. and Alva B. Gimbel Foundation.
520 K.L.G. is funded by an NIH National Institute on Drug Abuse (NIDA) grants R01DA046096 and
521 R01NS082413. K.A.E. is funded by NIH NIAMS grants (R01AR066082 and R01AR079220).
522 M.A.L. is supported by an NIH NIAMS grant K08NS120812.

523

524

525 **Figure Legends**

526

527 **Figure 1. Characterization of a myofiber-specific *Dmd* conditional knockout mouse. A.**
528 Schematic outlining the generation of myofiber-specific Dystrophin conditional knockout mice
529 (*Dmd*:HSA KO) by breeding our $Dmd^{flox52/Y}$ mice to human skeletal actin (*HSA*)-Cre transgenic
530 mice. Cre-mediated excision of *Dmd* exon 52 results in an out-of-frame disruption and instability
531 of the Dp427 RNA transcript. **B.** Western immunoblotting for the large Dp427m protein in the TA
532 and soleus muscles of WT (open), $Dmd^{flox52/Y}$ (blue), mdx^{5cv} (red), and *Dmd*:HSA KO (green) adult
533 (6-month-old) male mice. **C.** Densitometry graphs WT, $Dmd^{flox52/Y}$, mdx^{5cv}, and *Dmd*:HSA KO
534 immunoblots taken from TA and soleus muscle lysates and normalized to Vinculin protein. N = 5
535 separate mice per cohort. **D.** Histochemical staining of TA, soleus, and diaphragm muscles
536 isolated from the WT, $Dmd^{flox52/Y}$, mdx^{5cv}, and *Dmd*:HSA KO male mice. Hematoxylin and eosin
537 (H&E), picrosirius red, and Masson's trichrome histochemical staining performed. Scale bar = 100
538 µm. **E.** Percent fibrosis (%) in the TA muscles of the four mouse cohorts analyzed. **F.** Percentage
539 (%) centralized myonuclei for the approximately 600 myofibers of the TA muscles of the four
540 mouse cohorts analyzed. **G.** Cross-sectional area (CSA) displaying myofiber sizes (μm^2) shown
541 for each of the four cohorts. Two-way ANOVA with Bonferroni correction performed. P-values of
542 significance are shown: * $p < 0.05$, ** $p < 0.01$, *** $p < 0.005$, and **** $p < 0.001$.

543

544 **Figure 2. Adult *Dmd* myofiber KO mice have a poor running capacity. A.** Rotarod analysis
545 shown for the four mouse cohorts: WT, $Dmd^{flox52/Y}$, mdx^{5cv}, and *Dmd*:HSA KO. **B.** Grip strength
546 measured for mouse forelimbs shown normalized to grams (g) body weight. **C.** Open field testing
547 (OFT) of the four cohorts of mice showing distance traveled in centimeters (cm). **D.** and **E.** Forced
548 downhill treadmill running of the four cohorts of mice with average velocity and time to exhaustion
549 shown. N = 6 mice/cohort. Two-way ANOVA with Bonferroni correction performed. P-values of
550 significance are shown: * $p < 0.05$, ** $p < 0.01$, *** $p < 0.005$, and **** $p < 0.001$.

551

552 **Figure 3. *Dmd* myofiber KO muscles have disrupted cytokine and ECM signaling pathways.**
553 **A.** Volcano plot of the approximately 6,200 dysregulated DEGs in the TA muscles of *Dmd*:HSA
554 KO mice compared to $Dmd^{flox52/Y}$ (HSA-Cre-negative) aged-matched littermate controls. **B.** and **C.**
555 Heatmaps of significantly dysregulated showing significantly elevated (> 2.0 fold) or
556 downregulated (< 2.0 blue) DEGs with an emphasis on cytokine and ECM pathways. D. RNA-seq
557 DeSeq2 FKPM counts of three candidate highly disrupted transcripts that are validated DMD

558 muscle biomarkers: *Nos2*, *Col4a4*, and *Tgfb1* are shown. Four mice of each cohort (*Dmd*$^{flox52/Y}$-
559 black; *Dmd*:HSA KO- red) were analyzed for differentially expressed genes (DEGs). Student's t-
560 test, two tailed used for comparisons. P-values of significance are shown: * $p < 0.05$, ** $p < 0.01$,
561 *** $p < 0.005$, and **** $p < 0.001$.
562
563 **Figure 4. Postnatal loss of muscle dystrophin results in mild skeletal muscle pathologies.**
564 **A.** Schematic for conditional ablation of postnatal dystrophin using a tamoxifen-inducible (± TAM)
565 strategy. *Dmd*$^{flox52/Y}$ mice were mated to the *HSA*-MerCreMer (HSA-MCM) to conditionally ablate
566 dystrophin (+ TAM; red). *Dmd*:HSA (Cre+) mice given sunflower seed oil (- TAM) were used as
567 controls (black) After a one-week (5x per week) tamoxifen dosing (80 mg/kg body weight) in 8-
568 week-old male mice via intraperitoneal injection, mouse cohorts were evaluated at 0 (pre-dosing),
569 30, 60, 90, and 180 days (d) post deletion. N = 5 mice per cohort and time period for biopsy. **B.**
570 Densitometry western immunoblot measurements of the large dystrophin (Dp427m) protein
571 isoform measured in the TA, soleus, and diaphragm muscles. Note the robust persistence of the
572 large dystrophin protein and low protein turnover in the skeletal muscle tissues. **C.** H&E evaluation
573 of *Dmd*$^{flox52/Y}$:HSA-MCM (Cre+) mice (± TAM) evaluated at 180 days post ablation. Scale bar =
574 200 µm. **D.** and **E.** CSA and minimum Feret diameter measured at 180 days in the TA muscles
575 reveal smaller groupings of myofibers in the *md*$^{flox52/Y}$:HSA-MCM (Cre+) mice (+ TAM) mice
576 compared to (- TAM) controls. Student's t-test, two tailed used for comparisons. P-values of
577 significance are shown: * $p < 0.05$, ** $p < 0.01$, *** $p < 0.005$, and **** $p < 0.001$.
578
579 **Figure 5. Loss of Purkinje neuron brain *Dystrophin* impairs neurobehaviors in mice. A.**
580 Breeding schematic for the *Dmd*$^{flox52/Y}$ line to the *L7/Pcp2*-Cre (cerebellar Cre driver) transgenic
581 line to generate Dmd:Pcp2 KO mice. **B.** Densitometry western immunoblot quantification of the
582 large dystrophin (Dp427) protein expression in the cerebellum, cortex, and hypothalamus regions
583 of the brain in the *Dmd*$^{flox52/Y}$ (Cre-; open) and *Dmd*:Pcp2 KO (Cre+; grey) cohorts. N = 5 mice per
584 cohort were analyzed. **C.** Graphics showing the social approach (novel mouse versus novel
585 object) and social novelty (novel mouse versus familiar mouse) assays performed on the cohorts
586 of mice in a 3-chamber assay system. **D.** and **E.** Social approach and social novelty time in
587 chambers (1, 2, and 3) shown between the 3 analyzed mouse cohorts: the *Dmd*$^{flox52/Y}$ (open bars),
588 *Dmd*:Pcp2 KO (grey bars), and *mdx*^{5cv} (red bars). Time in chamber and time investigating in
589 minutes (mins) are shown. N = 10 mice per cohort were analyzed with an acclimation period of
590 equivalent amounts. **F.** and **G.** T- and Y-maze assessments of the 3 mouse cohorts are shown
591 with spontaneous alternation and the number of total arm visits. **H.** Morris water maze (MWM)

assessments in the 3 cohorts are shown as distance to platform (cm) compared to trial day. Spatial and reverse learning assessments were performed on separate days. N = 10 adult (6-month-old) mice were analyzed for each cohort. Two-way ANOVA with Bonferroni correction performed. P-values of significance are shown: * $p < 0.05$, ** $p < 0.01$, *** $p < 0.005$, and **** $p < 0.001$.

Supplementary Figure Legend

Supplemental Figure S1: Immunofluorescent confirmation of the loss of skeletal muscle dystrophin. Immunofluorescent imaging of the TA skeletal muscle and the DYS1 (Dp427 large isoform; purple) along with laminin (green) and DAPI (blue nuclei) co-labeling. Each of the four mouse cohorts are represented: WT, *Dmd*$^{flox52/Y}$, *mdx*^{5cv}, and *Dmd*:HSA KO. Scale bar = 100 µm. N = 5 adult (6-month-old) mice were analyzed for each cohort.

Supplemental Figure S2: Adult *Dmd* myofiber KO mice have physiological force deficits. A. Muscle mass (mg) taken from muscle biopsies from *Dmd*^{flox52}/Y (Cre-) (black) and *Dmd*$^{flox52/Y}$:HSA KO (Cre+) (red) mice shown. **B.** Absolute peak specific muscle force (mN). **C.** Normalized peak specific muscle force normalized to CSA (kPa). **D.** Post-eccentric contraction muscle force shown as relative force quantified over contraction number. **E.** Post eccentric relative force (mN) and Force-Frequency H values are shown between the cohorts. N = 10 mice per cohort. One way ANOVA with Bonferroni correction is shown. P-values of significance are shown: * $p < 0.05$, ** $p < 0.01$, *** $p < 0.005$, and **** $p < 0.001$; ns = non-significant.

Supplemental Figure S3: Conditional *Dmd* myofiber KO mice have impaired skeletal muscle regeneration. A. Histochemical evaluation of the TA muscles 14 and 21 days post cardiotoxin-induced skeletal muscle injury. H&E, picrosirius red, and Masson's trichrome staining of the TA muscles showing elevated areas of fibrosis, myofiber degeneration, and necrosis in the *Dmd*:HSA mKO mice at 14d and 21d post-ctx induced muscle injury compared to *Dmd*$^{flox52/Y}$ control mice. Scale bar = 100 µm. **B.** Laminin immunofluorescent imaging showing increased centralized myonuclei and smaller myofibers in the 14d and 21d post-ctx injured *Dmd*:HSA mKO mice. Scale bar = 80 µm. N = 5 mice per cohort.

Supplemental Figure S4: IPA pathway analysis of the conditional *Dmd* myofiber knockout mice. IPA analysis of the top dysregulated signaling pathways disrupted in the adult TA muscles

of the *Dmd*:HSA mKO mice compared to *Dmd*$^{flox52/Y}$ control mice. -log p-values shown with increased pathways (orange) and downregulated pathways (blue) shown.

Supplemental Figure S5: Confirmation of cerebellar dystrophin Dp427 protein knockdown in Dmd:Pcp2 isolated cerebellums. Western immunoblot analysis showing knockdown of cerebellar large dystrophin (Dp427c) in the isolated cerebellums of adult *Dmd*:Pcp2 KO mice. WT (*C57BL/6J*), *Dmd*$^{flox52/Y}$, and *Dmd*:Pcp2 KO mouse cohorts were analyzed. The Dp140 dystrophin isoform was also reduced in the *Dmd*:Pcp2 KO mouse cohorts. GAPDH levels were used to normalize protein lysates for comparative analyses.

References

1. M. Koenig *et al.*, Complete cloning of the duchenne muscular dystrophy (DMD) cDNA and preliminary genomic organization of the DMD gene in normal and affected individuals. *Cell* **50**, 509-517 (1987).
2. E. P. Hoffman, R. H. Brown, L. M. Kunkel, Dystrophin: the protein product of the Duchenne muscular dystrophy locus. *Cell* **51**, 919 - 928 (1987).
3. G. Bulfield, W. G. Siller, P. A. Wight, K. J. Moore, X chromosome-linked muscular dystrophy (mdx) in the mouse. *Proceedings of the National Academy of Sciences* **81**, 1189-1192 (1984).
4. P. Sicinski *et al.*, The molecular basis of muscular dystrophy in the mdx mouse: a point mutation. *Science* **244**, 1578-1580 (1989).
5. M. Rodrigues, Y. Echigoya, S.-i. Fukada, T. Yokota, Current Translational Research and Murine Models For Duchenne Muscular Dystrophy. *J Neuromuscul Dis* **3**, 29-48 (2016).
6. A. Bez Batti Angulski *et al.*, Investigations of an inducible intact dystrophin gene excision system in cardiac and skeletal muscle in vivo. *Scientific Reports* **10**, 10967 (2020).
7. E. Araki *et al.*, Targeted Disruption of Exon 52 in the Mouse Dystrophin Gene Induced Muscle Degeneration Similar to That Observed in Duchenne Muscular Dystrophy. *Biochemical and Biophysical Research Communications* **238**, 492-497 (1997).
8. A. Saoudi *et al.*, Emotional behavior and brain anatomy of the mdx52 mouse model of Duchenne muscular dystrophy. *Disease Models & Mechanisms* **14** (2021).
9. S. Shibuya *et al.*, Muscle Plasma Membrane Changes in Dystrophin Gene Exon 52 Knockout Mouse. *Pathology - Research and Practice* **197**, 441-447 (2001).
10. T. Oliver *et al.*, The glucocorticoid receptor acts locally to protect dystrophic muscle and heart during disease. *Disease Models & Mechanisms* **17** (2024).
11. Y. Hashimoto *et al.*, Brain Dp140 alters glutamatergic transmission and social behaviour in the mdx52 mouse model of Duchenne muscular dystrophy. *Progress in Neurobiology* **216**, 102288 (2022).
12. N. Beastrom *et al.*, mdx5cv Mice Manifest More Severe Muscle Dysfunction and Diaphragm Force Deficits than Do mdx Mice. *The American Journal of Pathology* **179**, 2464-2474 (2011).
13. R. Willmann *et al.*, Enhancing translation: Guidelines for standard pre-clinical experiments in mdx mice. *Neuromuscular Disorders* **22**, 43-49 (2012).

14. K. E. Wells *et al.*, Relocalization of neuronal nitric oxide synthase (nNOS) as a marker for complete restoration of the dystrophin associated protein complex in skeletal muscle. *Neuromuscular Disorders* **13**, 21-31 (2003).
15. Y. Lai *et al.*, Dystrophins carrying spectrin-like repeats 16 and 17 anchor nNOS to the sarcolemma and enhance exercise performance in a mouse model of muscular dystrophy. *The Journal of Clinical Investigation* **119**, 624-635 (2009).
16. J. A. Call, J. N. Mckeehen, S. A. Novotny, D. A. Lowe, Progressive resistance voluntary wheel running in the mdx mouse. *Muscle & Nerve* **42**, 871-880 (2010).
17. K. E. Schill *et al.*, Muscle damage, metabolism, and oxidative stress in mdx mice: Impact of aerobic running. *Muscle & nerve* **54**, 110-117 (2016).
18. M. S. Alexander *et al.*, Reversal of neurobehavioral social deficits in dystrophic mice using inhibitors of phosphodiesterases PDE5A and PDE9A. *Translational Psychiatry* **6**, e901-e901 (2016).
19. M. E. D. Stefano, V. Ferretti, C. Mozzetta, Synaptic alterations as a neurodevelopmental trait of Duchenne muscular dystrophy. *Neurobiology of Disease* **168**, 105718 (2022).
20. C. Vaillend, R. Chaussenot, Relationships linking emotional, motor, cognitive and GABAergic dysfunctions in dystrophin-deficient mdx mice. *Human Molecular Genetics* **26**, 1041-1055 (2017).
21. A. Saoudi *et al.*, Impact of distinct dystrophin gene mutations on behavioral phenotypes of Duchenne muscular dystrophy. *Disease Models & Mechanisms* **17** (2024).
22. J. W. McGreevy, C. H. Hakim, M. A. McIntosh, D. Duan, Animal models of Duchenne muscular dystrophy: from basic mechanisms to gene therapy. *Disease Models & Mechanisms* **8**, 195-213 (2015).
23. C. R. Heier *et al.*, The X-linked Becker muscular dystrophy (bmx) mouse models Becker muscular dystrophy via deletion of murine dystrophin exons 45–47. *Journal of Cachexia, Sarcopenia and Muscle* **14**, 940-954 (2023).
24. M. Ghahramani Seno *et al.*, Transcriptomic analysis of dystrophin RNAi knockdown reveals a central role for dystrophin in muscle differentiation and contractile apparatus organization. *BMC Genomics* **11**, 345 (2010).
25. M. R. F. Gosselin *et al.*, Loss of full-length dystrophin expression results in major cell-autonomous abnormalities in proliferating myoblasts. *eLife* **11**, e75521 (2022).
26. In Y. Choi *et al.*, Concordant but Varied Phenotypes among Duchenne Muscular Dystrophy Patient-Specific Myoblasts Derived using a Human iPSC-Based Model. *Cell Reports* **15**, 2301-2312 (2016).
27. L. Caputo *et al.*, Acute conversion of patient-derived Duchenne muscular dystrophy iPSC into myotubes reveals constitutive and inducible over-activation of TGFβ-dependent pro-fibrotic signaling. *Skeletal Muscle* **10**, 13 (2020).
28. J. Massenet *et al.*, Epigenetic control of myogenic identity of human muscle stem cells in Duchenne Muscular Dystrophy. *bioRxiv* 10.1101/2023.04.26.538414, 2023.2004.2026.538414 (2023).
29. Y. Liu *et al.*, PTPN1/2 inhibition promotes muscle stem cell differentiation in Duchenne muscular dystrophy. *Life Science Alliance* **8**, e202402831 (2025).
30. F. Yue *et al.*, PTEN Inhibition Ameliorates Muscle Degeneration and Improves Muscle Function in a Mouse Model of Duchenne Muscular Dystrophy. *Molecular Therapy* **29**, 132-148 (2021).
31. M. S. Alexander *et al.*, MicroRNA-486–dependent modulation of DOCK3/PTEN/AKT signaling pathways improves muscular dystrophy–associated symptoms. *The Journal of Clinical Investigation* **124**, 2651-2667 (2014).
32. N. A. Dumont *et al.*, Dystrophin expression in muscle stem cells regulates their polarity and asymmetric division. *Nat Med* **21**, 1455-1463 (2015).

33. Y. X. Wang *et al.*, EGFR-Aurka Signaling Rescues Polarity and Regeneration Defects in Dystrophin-Deficient Muscle Stem Cells by Increasing Asymmetric Divisions. *Cell Stem Cell* 10.1016/j.stem.2019.01.002 (2019).
34. K. Kodippili, M. A. Rudnicki, Satellite cell contribution to disease pathology in Duchenne muscular dystrophy. *Frontiers in Physiology* **14** (2023).
35. U. Gurriaran-Rodriguez *et al.*, Wnt7a is Required for Regeneration of Dystrophic Skeletal Muscle. *bioRxiv* 10.1101/2024.01.24.577041, 2024.2001.2024.577041 (2024).
36. C. Pascual-Morena *et al.*, Dystrophin Genotype and Risk of Neuropsychiatric Disorders in Dystrophinopathies: A Systematic Review and Meta-Analysis. *J Neuromuscul Dis* **10**, 159-172 (2023).
37. M. Thangarajh *et al.*, Relationships between DMD mutations and neurodevelopment in dystrophinopathy. *Neurology* **93**, e1597-e1604 (2019).
38. M. Thangarajh *et al.*, Neurodevelopmental Needs in Young Boys with Duchenne Muscular Dystrophy (DMD): Observations from the Cooperative International Neuromuscular Research Group (CINRG) DMD Natural History Study (DNHS). *PLoS currents* **10**, ecurrents.md.4cdeb6970e54034db54032bc54033dfa54054b54034d54987 (2018).
39. W.-C. Wu, S. P. Bradley, J. M. Christie, J. R. Pugh, Mechanisms and Consequences of Cerebellar Purkinje Cell Disinhibition in a Mouse Model of Duchenne Muscular Dystrophy. *The Journal of Neuroscience* **42**, 2103-2115 (2022).
40. T. L. Stay, L. N. Miterko, M. Arancillo, T. Lin, R. V. Sillitoe, In vivo cerebellar circuit function is disrupted in an mdx mouse model of Duchenne muscular dystrophy. *Disease Models & Mechanisms* 10.1242/dmm.040840, dmm.040840 (2019).
41. R. Chaussenot *et al.*, Cognitive dysfunction in the dystrophin-deficient mouse model of Duchenne muscular dystrophy: A reappraisal from sensory to executive processes. *Neurobiology of Learning and Memory* **124**, 111-122 (2015).
42. F. Zarrouki *et al.*, Partial Restoration of Brain Dystrophin and Behavioral Deficits by Exon Skipping in the Muscular Dystrophy X-Linked (mdx) Mouse. *Annals of Neurology* **92**, 213-229 (2022).
43. C. Vaillend *et al.*, Rescue of a Dystrophin-like Protein by Exon Skipping In Vivo Restores GABAA-receptor Clustering in the Hippocampus of the mdx Mouse. *Mol Ther* **18**, 1683-1688 (2010).
44. C. Wang, F. Yue, S. Kuang, Muscle Histology Characterization Using H&E Staining and Muscle Fiber Type Classification Using Immunofluorescence Staining. *Bio Protoc* **7** (2017).
45. L. A. Riley *et al.*, The skeletal muscle circadian clock regulates titin splicing through RBM20. *eLife* **11**, e76478 (2022).
46. B. D. Harfmann *et al.*, Muscle-specific loss of Bmal1 leads to disrupted tissue glucose metabolism and systemic glucose homeostasis. *Skeletal Muscle* **6**, 12 (2016).
47. A. L. Reid *et al.*, DOCK3 is a dosage-sensitive regulator of skeletal muscle and Duchenne muscular dystrophy-associated pathologies. *Human Molecular Genetics* **29**, 2855-2871 (2020).
48. Y. M. Kobayashi, E. P. Rader, R. W. Crawford, K. P. Campbell, Endpoint measures in the mdx mouse relevant for muscular dystrophy pre-clinical studies. *Neuromuscular Disorders* **22**, 34-42 (2012).
49. M. Yang, J. L. Silverman, J. N. Crawley, "Automated Three-Chambered Social Approach Task for Mice" in Current Protocols in Neuroscience. (John Wiley & Sons, Inc., 2011).
50. C. Vaillend, A. Rendon, R. Misslin, A. Ungerer, Influence of dystrophin-gene mutation on mdx mouse behavior. I. Retention deficits at long delays in spontaneous alternation and bar-pressing tasks. *Behav Genet* **25**, 569-579 (1995).

51. S. Engelbeen, A. Aartsma-Rus, B. Koopmans, M. Loos, M. van Putten, Assessment of Behavioral Characteristics With Procedures of Minimal Human Interference in the mdx Mouse Model for Duchenne Muscular Dystrophy. *Frontiers in Behavioral Neuroscience* **14** (2021).
52. M. Verhaeg *et al.*, Learning, memory and blood–brain barrier pathology in Duchenne muscular dystrophy mice lacking Dp427, or Dp427 and Dp140. *Genes, Brain and Behavior* **23**, e12895 (2024).
53. C. V. Vorhees, M. T. Williams, Morris water maze: procedures for assessing spatial and related forms of learning and memory. *Nature Protocols* **1**, 848-858 (2006).
54. J. Köster, S. Rahmann, Snakemake—a scalable bioinformatics workflow engine. *Bioinformatics* **28**, 2520-2522 (2012).
55. A. Krämer, J. Green, J. Pollard, S. Tugendreich, Causal analysis approaches in Ingenuity Pathway Analysis. *Bioinformatics* **30**, 523-530 (2014).

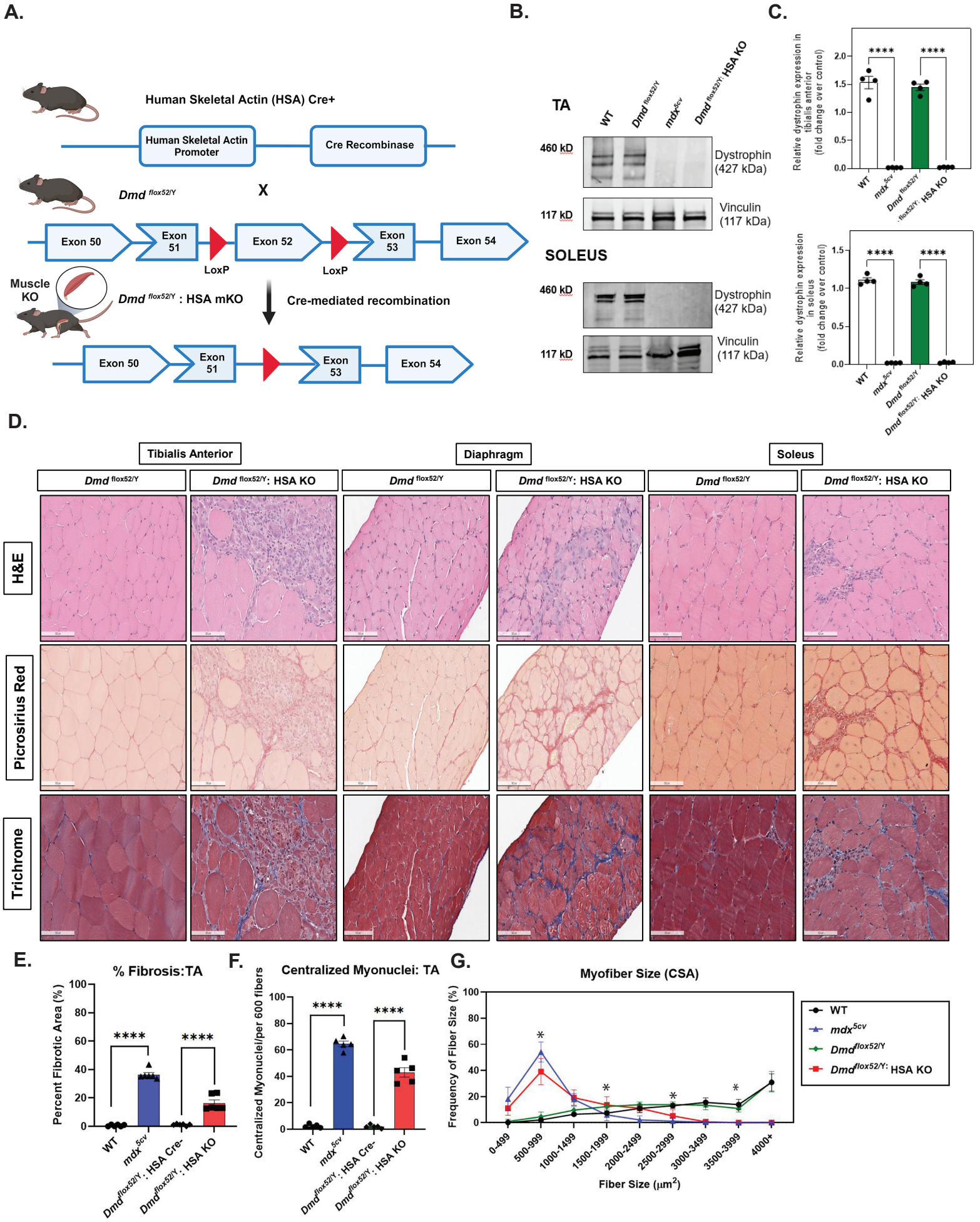

Figure 1. Characterization of a myofiber-specific *Dmd* conditional Dmd knockout mouse.

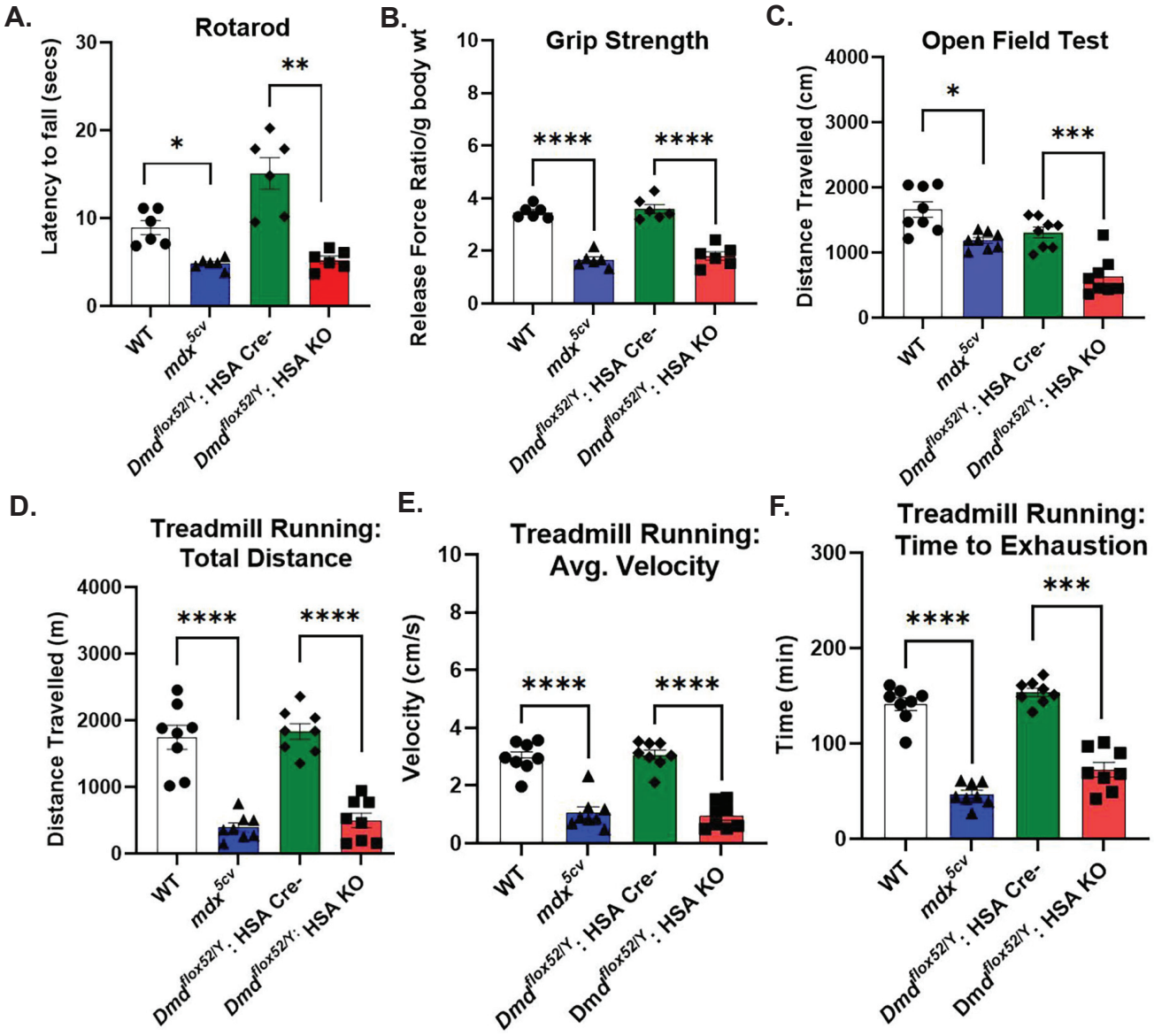

Figure 2: Adult *Dmd* myofiber KO mice have a poor running capacity.

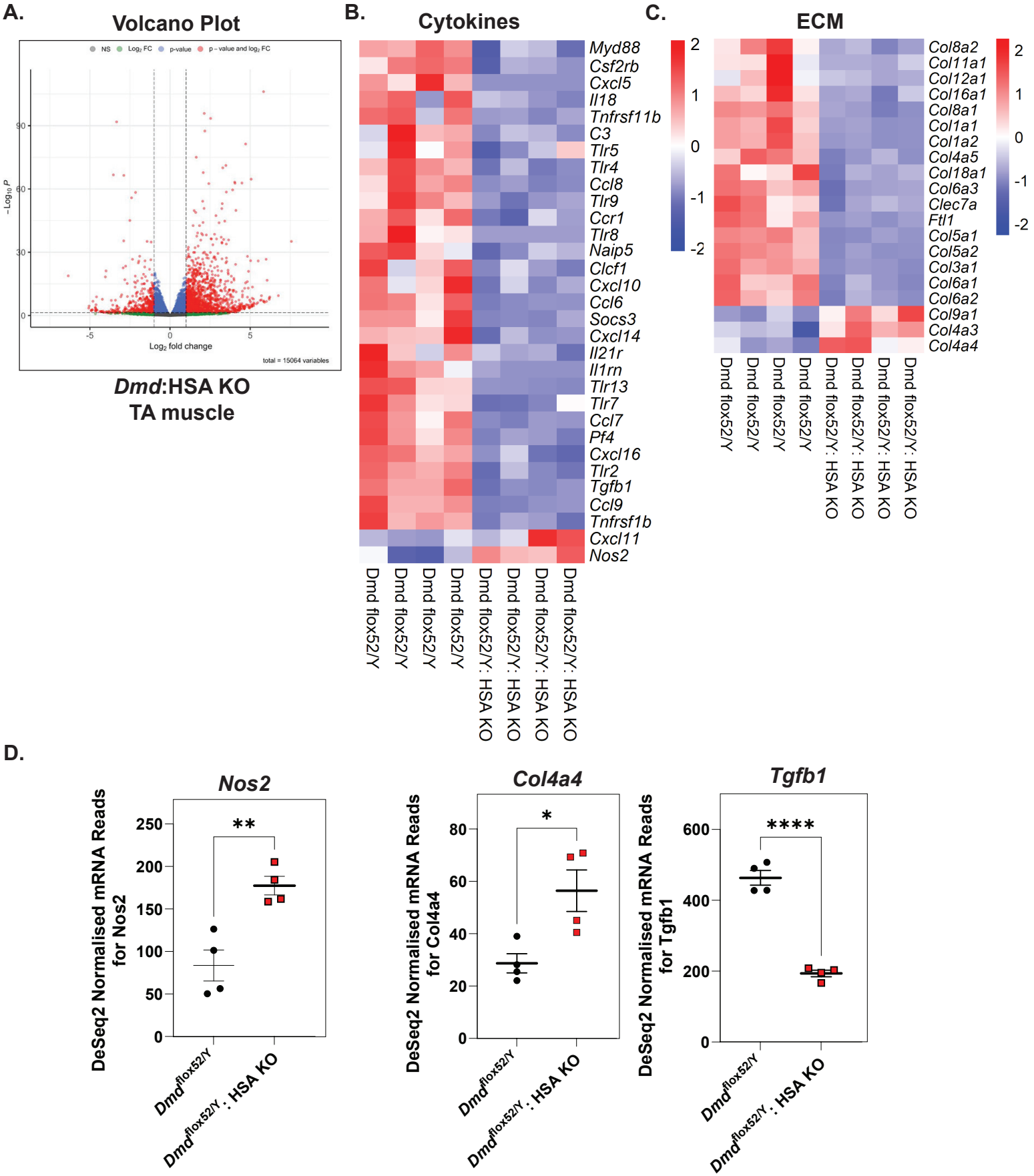

Figure 3: *Dmd* myofiber KO muscles have disrupted cytokine and ECM signaling pathways.

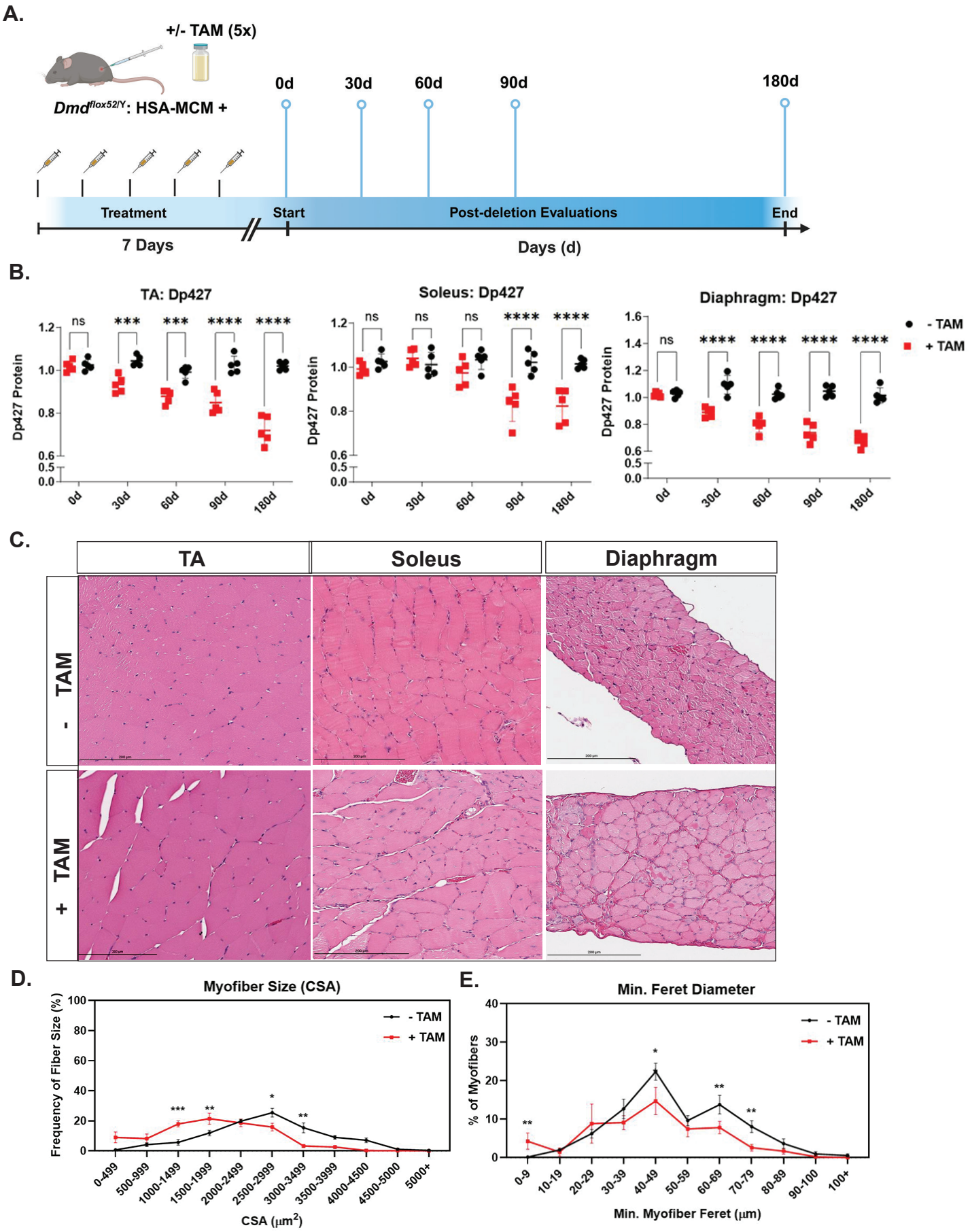

Figure 4. Postnatal loss of muscle dystrophin results in a mild skeletal muscle pathologies.

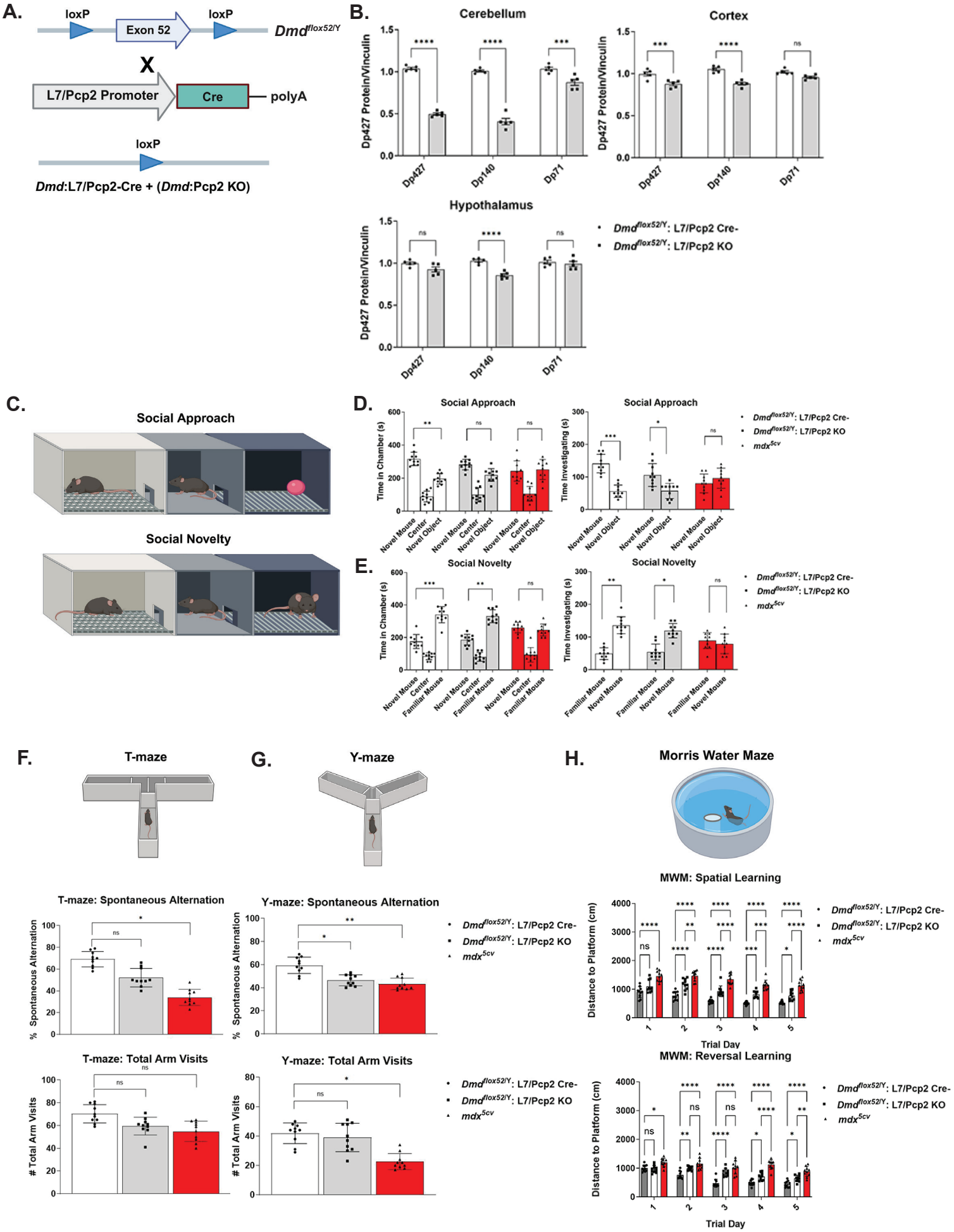

Figure 5. Loss of Purkinje neuron brain *Dystrophin* impairs neurobehaviors in mice.